journal

J. Am. Ceram. Soc., 94 [10] 3340–3345 (2011)
DOI: 10.1111/j.1551-2916.2011.04614.x

Preparation and Characterization of $(La_{0.8}Sr_{0.2})_{0.95}MnO_{3-\delta}$ (LSM) Thin Films and LSM/LSCF Interface for Solid Oxide Fuel Cells

Jong-Jin Choi,[‡,§] Wantao Qin,[‡] Mingfei Liu,[‡] and Meilin Liu[‡,†]

[‡]School of Materials Science and Engineering, Georgia Institute of Technology, Atlanta, GA, 30332-0245, USA

[§]Functional Ceramics Group, Korea Institute of Materials Science, 797 Changwondaero, Sungsan-gu, Changwon, Gyeongnam, 642-831, Korea

Uniform, dense, and conformal coatings of (La,Sr)$MnO_{3-\delta}$ (LSM) have been successfully deposited on a silicon wafer and a dense (La,Sr)(Co,Fe)$O_{3-\delta}$ (LSCF) substrate using a stable LSM sol consisting of metal acetate and nitrate precursors dissolved in a mixed organic solvent of 2-methoxyethanol and acetic acid with enhanced wettability. The processing conditions are optimized for precise control of composition, morphology, microstructure, and thickness of the LSM films to examine the microstructure and chemical stability of an LSM film as a catalytic coating for an LSCF cathode. The thicknesses of the LSM films are controlled within the range of 5–60 nm by spin-coating of LSM sol with different concentrations. The LSM films grow epitaxially on the LSCF substrate grains after annealing at 800°C for 1 h due to their structural similarity. The LSM coatings show good stability on LSCF substrates and may suppress strontium oxide segregation on LSCF surface during annealing at 850°C for 900 h, implying that LSM-coated LSCF surfaces have better structural and chemical stability under typical fuel cell operating conditions.

I. Introduction

A solid oxide fuel cell (SOFC) represents the cleanest, most efficient and versatile chemical-to-electrical energy conversion system. One of the critical challenges in the commercialization of SOFC is to develop cells that can operate at sufficiently low temperatures to reduce the cost and improve the reliability.[1,2] Among the parts of a SOFC stack, the cathode plays an important role because most of the power losses arise from the cathode relevant to oxygen reduction, more so at lower operation temperatures.[3,4] (La,Sr)$MnO_{3-\delta}$ (LSM) is one of the most widely used cathode materials owing to its high electrochemical activity for oxygen reduction, good stability, and compatibility with the yttria stabilized zirconia (YSZ) electrolyte. However, the performances of an LSM cathode are limited severely by its poor oxygen ion conductivity at low temperatures ($\leq$700°C). In contrast, (La,Sr)(Co,Fe)$O_{3-\delta}$ (LSCF) perovskite oxides have been widely used as cathode materials for SOFC to enhance the cathode performance at reduced temperatures because of their excellent ionic and electronic conductivities which may potentially expand the active site from three-phase boundaries (TPBs) to the entire surface of LSCF.[5,6]

Even though cells with LSCF cathodes show significantly higher power densities than those with LSM cathodes, long-term stability of LSCF cathodes is still a concern.[7] Degradation of 0.06%–0.17% of power density per hour has been reported for the anode-supported YSZ cells with LSCF cathode operated at 750°C and 0.7 V.[7,8] The most obvious downfall of LSCF is that it reacts adversely with YSZ electrolyte, which can be mitigated by the use of a buffer layer of doped-CeO_2 between LSCF and YSZ.[7] Additionally, Sr-enrichment on the LSCF surface was proposed as a cause of LSCF performance degradation.[7,9,10]

Another limitation of LSCF cathode for the performance maximization is its surface catalytic activity. The electrochemical activity of the stand-alone LSCF cathode is likely to be limited by the surface catalytic properties.[11–13] On the other hand, LSM cathode is known to have strong oxygen adsorption characteristics with rapid catalytic kinetics[14] as well as higher chemical stability, which can help overcome the electrochemical and chemical limitation of the LSCF cathode. Therefore, higher electrochemical performance with enhanced long-term stability is expected when the LSCF surface is modified by a thin LSM film (probably less than 50-nm thick). Improved performance and stability of the LSM-coated LSCF cathode has been reported in our previous work[15]; however, the detailed microstructure and chemical stability of the LSM/LSCF interface have not yet been reported.

In this study, we report our findings in preparation and characterization of LSM thin films on silicon wafers and dense LSCF substrates using a sol–gel process for precise control of morphology, microstructure, composition, and thickness of LSM films. Further, to observe the evolution of microstructure, composition, and morphology of the LSM films on LSCF surfaces as well as the LSM/LSCF interfaces, we examined the annealed LSM-coated dense LSCF electrode samples under conditions similar to fuel cell operation for ~900 h.

II. Experimental Procedure

The target composition for the LSM films is $(La_{0.8}Sr_{0.2})_{0.95}MnO_3$, creating ~5% of A-site deficiency in the ABO_3 compound to enhance the long-term electrochemical stability of the LSM film.[16] The LSM sols with concentrations of 0.05, 0.10, and 0.30M (mol/L) were prepared by dissolving proper amounts of $La(NO_3)_3{\cdot}6H_2O$, $Sr(CH_3COO)_2$, $Mn(CH_3COO)_2{\cdot}4H_2O$ (all 99.9%, Aldrich Chemical Co., Milwaukee, WI, USA) in different mixed solvents at room temperature (~25°C). Many solvents were examined in this study, including ethanol, *i*-propanol, *n*-propanol, ethylene glycol, 1,3-propanediol, 2-methoxyethanol, and acetic acid (all >99.9%, Aldrich Chemical Co., Milwaukee, WI, USA). Among them, a mixed solvent of 2-methoxyethanol and acetic acid appears the best. The volume fraction of acetic acid in the solvent mixture was varied from 0 to 2/3, with 1/

J. Stevenson—contributing editor

Manuscript No. 29176. Received January 12, 2011; approved April 08, 2011.
†Author to whom correspondence should be addressed. e-mail: meilin.liu@mse.gatech.edu

3 being the best to optimize the stability and wettability of the sol. The prepared sol was aged for 1 day before it was coated on the substrate. A small amount of the sol was dried at 100°C for 12 h and calcined at 600°–800°C for 1 h to produce powder samples for confirmation of phase formation.

Dense pellets of $La_{0.6}Sr_{0.4}Co_{0.2}Fe_{0.8}O_{3-\delta}$ (LSCF) were prepared by dry-pressing (10 mm diameter, 300 MPa) of LSCF powders (prepared by either solid state reaction or a sol–gel process) and subsequent sintering at 1350°C for 7 h in an oxygen atmosphere. One side of each sintered LSCF pellet was ground and polished down to 1 μm using a diamond paste, cleaned, and thermally annealed at 1080°C for 2 h before deposition of LSM thin films.

The LSM stock solutions of different concentrations were deposited onto the commercially available glass slides and silicon wafers using a spin-coater at 3000 rpm for different periods of time, after which the uniformity, thickness, and phase formation of LSM films would be evaluated. Optimized deposition parameters were then applied to the deposition of LSM films on LSCF pellets. The deposited films were pyrolyzed at 300°C for 10 min on a digitally controlled hot-plate and subsequently annealed at 600°–800°C for 1 h for the films on Si wafer pieces and at 900°C for 1 h for the films on LSCF pellets, in an electric furnace with a heating rate of 3°C/min. The annealing at the higher temperature of 900°C would allow the films to develop a more stable structure on the LSCF substrates. Further, some of the LSM films on LSCF pellets were annealed at 850°C for 900 h for the study of long-term stability and microstructural evolution of the surface and the LSM/LSCF interface under conditions similar to those of fuel cell operation.

The phases of the LSM powder and films were characterized by XRD (X'Pert Pro Alpha-1) using a *CuK*α radiation. Microanalyses of the LSM films and LSM/LSCF interface were performed using thermally assisted FE-SEM (LEO 1530: Geminil Zeiss, Oberkochen, Germany) and TEM/STEM/EDS (HF-3300; Hitachi, Japan) equipped with a field emission gun and operated at 300 kV. STEM and EDS were conducted with an electron probe of a size of about 5×10^{-1} nm. The TEM samples were prepared using a Hitachi NB5000 FIB-SEM operated at 40 kV.

III. Results and Discussion

(1) Stability and Wettability of LSM Sol

To characterize the stability of a thin LSM film on an LSCF substrate and the LSM/LSCF interface during SOFC operation, both the LSM film and the LSCF substrate should have precisely controlled stoichiometry and uniform composition. For the film prepared by a solution-based process, both the stoichiometry and composition distribution inside the film depend strongly on the chemical stability of each precursor in the solution. This is because a less stable precursor tends to precipitate first, resulting in composition inhomogeneity or phase segregation.

In this study, precursors (i.e., metal acetates/nitrate) for LSM sol were dissolved in a non-aqueous mixed solvent to optimize the stability and wettability of the sol on LSCF substrates. While water is an excellent solvent for most metal nitrates and acetates due to its high polarity and thus good solubility, its high surface tension (>70 mN/m) degrades the wettability of the solution. In contrast, the surface tensions of 2-methoxyethanol and acetic acid are 30.8 and 26.9 mN/m, respectively,[17] both of which are much lower than that of water. The solubilities of strontium acetate and manganese acetate in 2-methoxyethanol and acetic acid, respectively, are relatively high. Therefore, a mixture of the two solvents are ideally suitable for an LSM sol with high stability and wettability (the solubility of lanthanum nitrate is high enough in either solvent).

Because the strontium acetate shows higher solubility in 2-methoxyethanol than acetic acid and manganese acetate has higher solubility in acetic acid than 2-methoxyethanol, the ratio of the two solvents critically influences the stability of the LSM sol, more so at higher LSM concentration. The stability was determined by carefully monitoring precipitation after a 1-week aging of LSM solutions with different volume fractions of acetic acid and LSM concentrations, at room temperature (~25°C). The LSM sol with acetic acid volume fraction of 1/3 (or volume ratio of 2-methoxyethanol to acetic acid =2:1) showed the highest stability in the LSM concentration range studied. For example, the 0.30M LSM sol with the optimum solvent ratio remained transparent without any precipitation after 6 months of aging at room temperature (~25°C). The LSM coatings derived from the non-aqueous acetate sol showed excellent wettability on Si wafer and LSCF pellet, while those derived from an aqueous nitrate sol (developed for infiltration into a porous structure[18]) showed poor wettability.

The minimum temperature required for the formation of the perovskite phase of LSM was estimated based on X-ray diffraction (XRD) analysis of the LSM powder samples derived from a 0.30M LSM sol and subsequently fired at different temperatures. The XRD patterns shown in Fig. 1 indicated that the desired perovskite phase was formed at 700°C, with small peaks of un-reacted phases at 25–26°. After annealing at 800°C for 1 h, however, all such small peaks of un-reacted phases disappeared, resulting in a single-phase perovskite of LSM.

(2) Optimization of Deposition Conditions

The thicknesses of the LSM film is critical to fundamental study of oxygen reduction processes.[19] As a catalytic coating, the thickness of LSM has to be less than 50 nm to be catalytically active and the observable catalytic activity varies sensitively with thickness. The thicknesses of LSM films derived from the spin-coating were controlled by the concentrations of the LSM sols and the number of coatings at a constant speed of rotation. A Si wafer (instead of an LSCF pellet) was first used as the substrate to facilitate the refinement of deposition conditions, since optically LSM films appear distinctly different from the Si wafer, which provided the ease for the assessment of the LSM films. Further, the large difference between the Si and LSM lattices greatly facilitated XRD identification of LSM crystalline phases on Si since they have distinctly different diffraction patterns. In contrast, an LSM film on an LSCF substrate would be diffi-

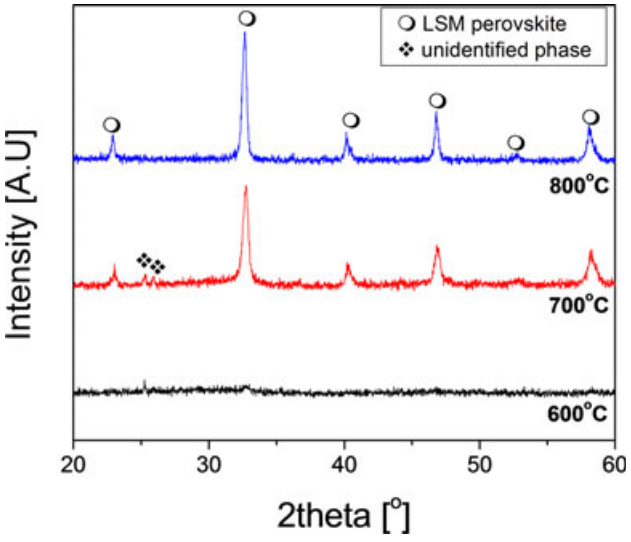

Fig. 1. XRD spectra of LSM powders derived from the 0.3M LSM sol with different calcination temperatures.

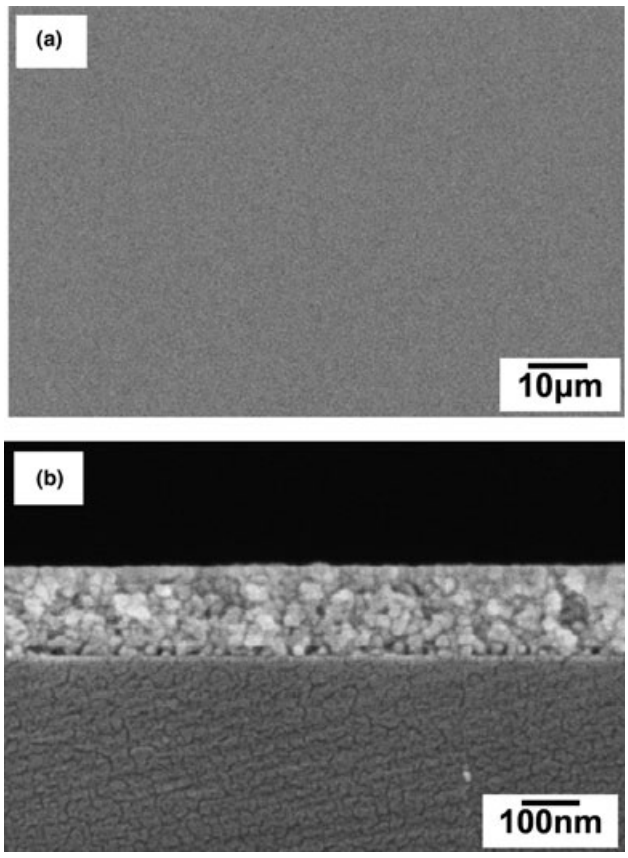

Fig. 2. (a) Top-down and (b) cross-sectional view (SEM micrographs) of an LSM film on Si wafer derived from three coatings of 0.30M LSM sol.

cult to identify since they appear similar under a microscope and their diffraction patterns are also nearly identical.

The deposition process is described as follows: first, the thicknesses of LSM films were controlled by sol concentration and repeating times of the spin-coating, with the rotation speed of the spin-coater being kept at 3000 rpm. The films were annealed at 800°C for 1 h and the LSM films on silicon substrate were examined using an optical microscope. As shown in Fig. 2(a), there were no observable cracks or large defects on the surface of an annealed LSM film using 0.30M LSM sol, similar to other films derived from LSM sols with different concentrations and different numbers of coatings (up to ~200 nm thickness). Shown in Fig.2 (b) is a cross-sectional SEM image of the same LSM film. The thickness of the uniform film is ~180 nm (three coatings at 3000 rpm). The thickness of the LSM film derived from five coatings of 0.10M sol is ~100 nm. Because the coating thickness is approximately proportional to the number of coatings, the thickness of the film derived from one coating of the 0.10M LSM sol is ~20 nm. Similarly, the thickness of the LSM film derived from one coating of the 0.02M LSM sol is ~5 nm.

The crystallization temperature and phase purity of the LSM film on Si wafer were studied with XRD, as shown in Fig. 3. The XRD patterns for the LSM film (~60 nm thick, from 0.30M LSM sol) annealed at different temperatures for 1 h are shown in Fig 3(a), which indicate that crystallinity at 600°C was below detection; in contrast, the (110) peak of the LSM perovskite phase near 32.5° appeared at 700°C, and all major peaks of the perovskite structure emerged at 800°C. Figure 3(b) shows XRD patterns of the LSM films annealed at 800°C for 1 h with different LSM sol concentrations and coating times. The patterns show that the peak intensities increase with concentration of the solution and film thickness.

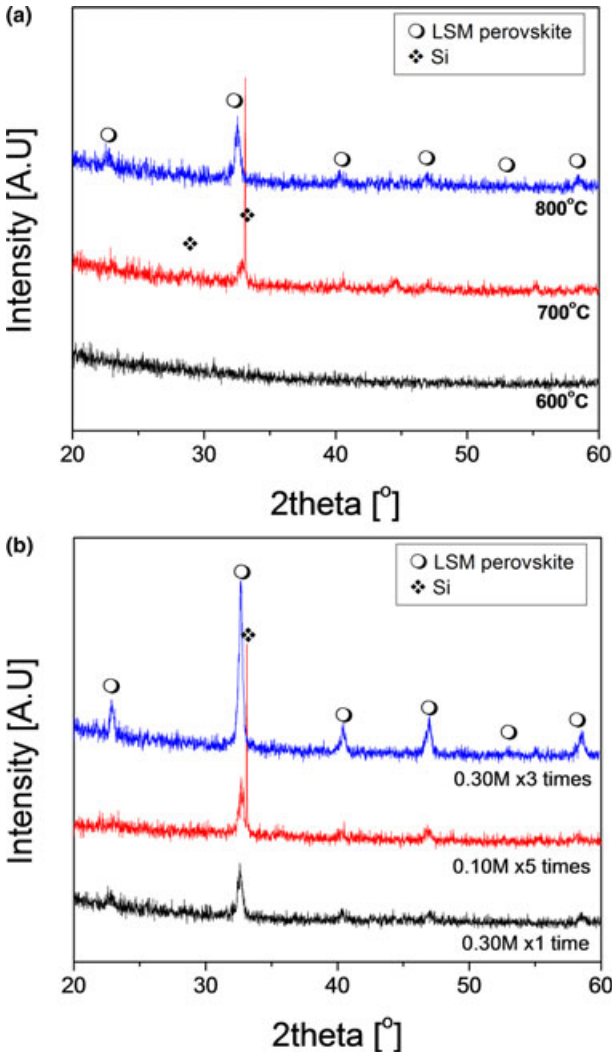

Fig. 3. XRD spectra of LSM films on Si wafer with different annealing temperatures (a) and different thicknesses and annealed at 800°C (b).

Figure 4 shows SEM images of the LSM films coated using 0.30M LSM sol (~60 nm thick) on a Si substrate and annealed at different temperatures. The film annealed at 600°C appears quite uniform. At 700°C, however, the homogeneity became lost and features in the size scale of a few tens of nanometer emerged. At 800°C, sizes of such features became larger and visibility higher. Correlating the SEM observation with the XRD patterns shown in Fig. 3(a), we believe that the surface features are images of either LSM grains or agglomerates of LSM grains, and the feature size increase seen in the SEM image indicates the increase of the grain size, which agrees well with the peak intensity increase observed in XRD.

(3) LSM Coatings on Dense and Flat LSCF Substrates

Once the processing conditions had been optimized on Si wafer, they were applied to fabricate LSM films on polished surfaces of LSCF pellets for the study of microstructure and phase stabilities of LSM film and LSM/LSCF interface. In contrast to the LSM films on Si substrates, LSM films were epitaxially grown on LSCF due to the structural similarity. Each of the LSM film on LSCF was annealed for 1 h at 900°C, slightly higher than SOFC operation temperatures (~750°C). Figure 5 shows XRD spectra of an LSCF pellet and LSM film on LSCF pellets, where the peak positions in the spectra almost coincide. This is due to the structure similarity of LSM and LSCF.[20]

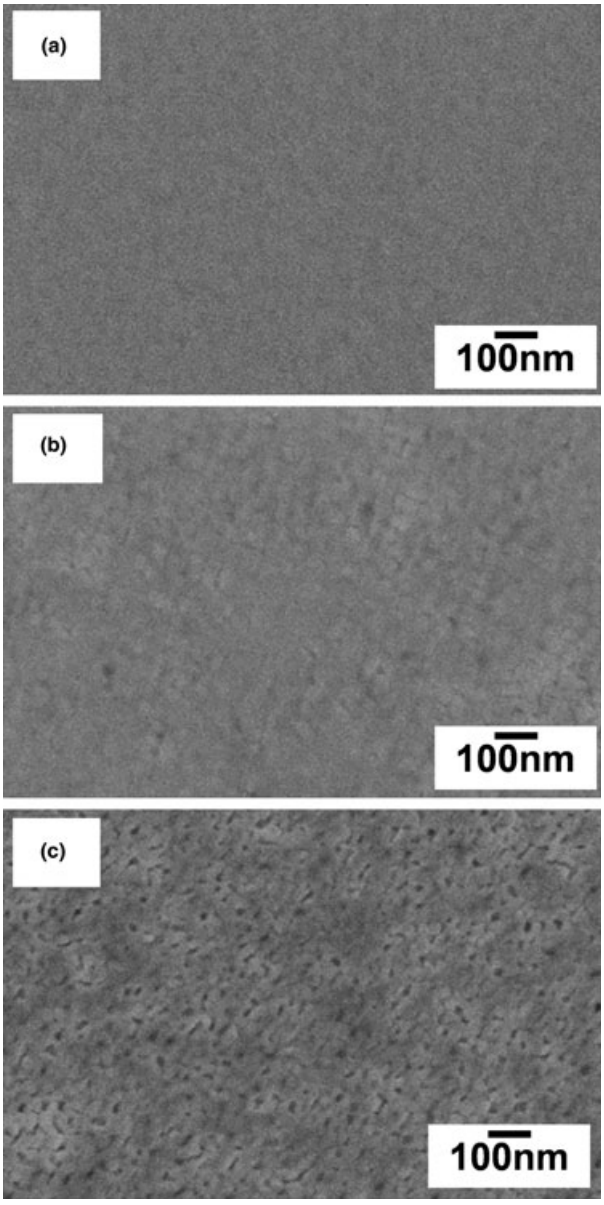

Fig. 4. Top-down SEM images of LSM films coated using 0.30M LSM sol on Si wafer with different annealing temperatures; (a) 600°C, (b) 700°C, and (c) 800°C for 1 h.

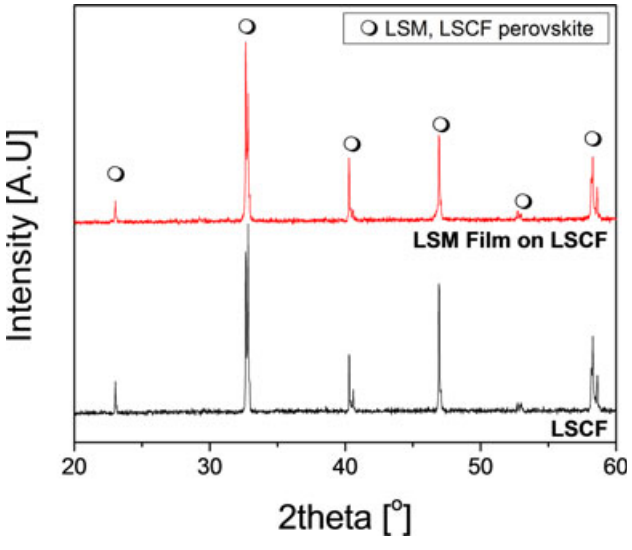

Fig. 5. XRD spectra of bare LSCF pellet and LSCF pellet coated with 0.30M LSM film.

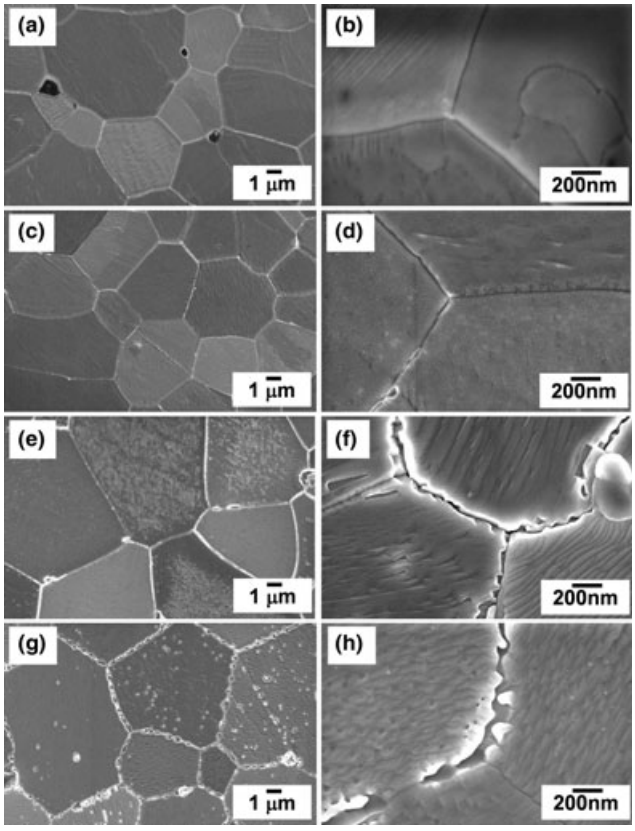

Fig. 6. SEM micrographs of bare LSCF pellet (a) & (b), and LSM films coated on LSCF pellets with different sol concentrations of 0.02M (c) & (d), 0.10M (e) & (f), and 0.30M (g) & (h).

Surface morphologies of a bare LSCF pellet and LSM-coated LSCF pellets prepared using LSM sols with different concentrations are shown in Fig.6. Grains of the bare LSCF pellet are visible in figures (a) and (b). The LSCF pellet coated with the 0.02M LSM sol appears almost identical to the bare LSCF pellet. This is because the LSM film is very thin (probably less than 5 nm thick), and the LSM film is expected to have become epitaxial to the underlying LSCF grains, The LSM films derived from the 0.10M and the 0.30M sols begin to display higher contrast across grain boundaries. The contrast from grain to grain is due probably to the different orientation of the LSM films inherited from the underlying LSCF grains. As will be seen in the following discussion, the LSM film is crystalline and epitaxial on LSCF.

The epitaxial structure of LSM film was confirmed by TEM analysis. Figure 7 is a montage of cross-sectional views (TEM images) of an LSM-coated LSCF pellet. The LSM film, derived from one coating of the 0.30M LSM, has a thickness ranging from 42 to 50 nm. HRTEM images of the LSM surface and LSM/LSCF interface are presented in Figs. 7(b) and (d), respectively, with the broken yellow line in the Fig. 7(b) marking the approximate median of the interface. Structural coherence between the two phases is shown by the complete alignment of lattice fringes of the two phases at their interface. Such an epitaxial growth of LSM on LSCF is attributed to the almost identical lattice structures of the two phases. Zone axis images of the surface of the LSM film and the two phases along their interface, processed after Fourier-filtering, are presented in Figs.7(c), (e), and (f), respectively. The LSM maintains a single crystal structure throughout the film thickness, which is manifested by the identical zone axes labeled for the top and bottom portions of the film and presented in figures (c) and (e), respectively.

Atomic percentage profiles across the LSM film and the LSM/LSCF interfaces, as determined using EDS attached to

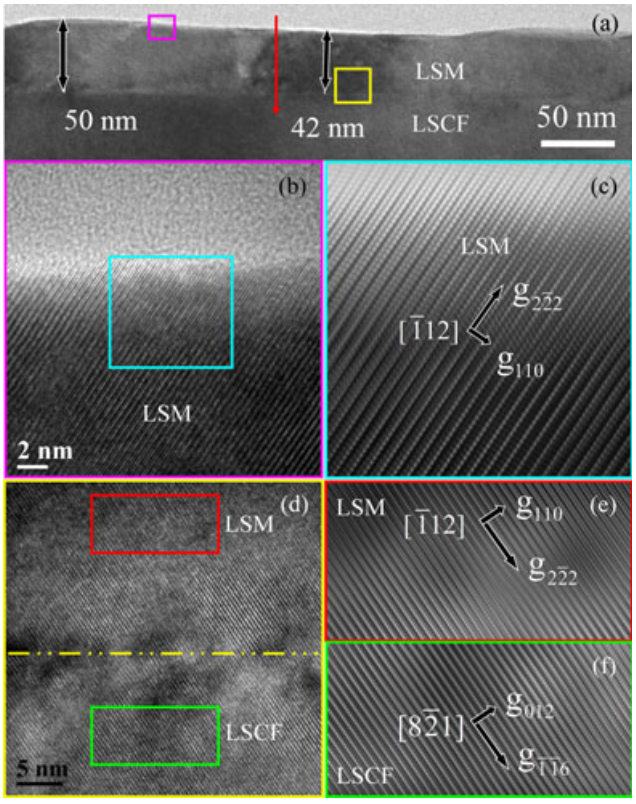

Fig. 7. TEM image of an LSM film (derived from a sol–gel process) on an LSCF pellet (a). The red arrow marks the profile line for the profiles presented in Fig. 8. HRTEM images of the LSM surface (b) and LSM-LSCF interface (d). Approximate medium of the interface is indicated by the broken yellow line in (d). (c), (e) and (f) are Fourier-filtered images of the LSM surface, LSM and LSCF near the interface, in the areas marked by the light blue rectangle in (b), and red and green rectangles in (d).

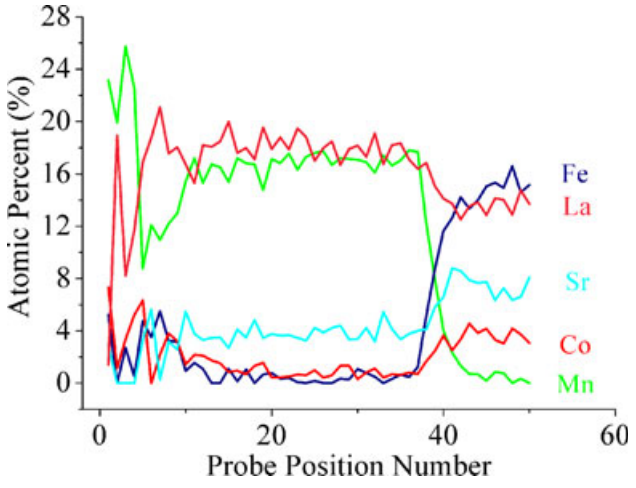

Fig. 8. Composition profiles across the LSM layer on the LSCF pellet.

the TEM, are presented in Fig. 8. The profiles show relatively uniform composition distribution inside the LSM film. The crossing point of the Fe and Mn profiles marks the approximate LSM/LSCF interface. Composition of the LSM film, acquired based on standardless quantification and shown in Fig. 8, approximately match the intended stoichiometry of the LSM film. Therefore, it is believed that no serious reaction occurred during film deposition and annealing steps.

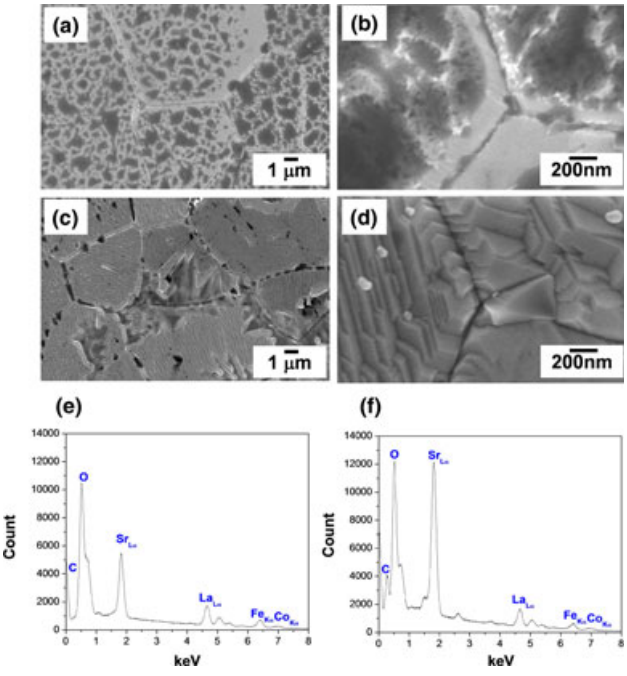

Fig. 9. Top-down SEM micrographs of the bare LSCF and 0.30M LSM-coated LSCF after annealing at 850°C for 900 h; (a),(b) bare LSCF pellets, (c),(d) LSM-coated LSCF. EDS spectra of the surface of the bare LSCF after annealing at 850°C for 900 h from (e) a white area (f) a dark area.

(4) Stability of the LSM Film and LSM/LSCF Interface

The bare LSCF and LSM-coated LSCF pellets were annealed at 850°C for 900 h for the study of the microstructural and chemical stabilities of the LSM film and LSM/LSCF interface after long-term operation at SOFC operation temperatures. Figure 9 shows the surfaces of a bare LSCF and an LSCF pellet coated with 0.30M LSM after annealing at 850°C for 900 h. For the bare LSCF, high local contrast over the size scale of tenths to several microns within each grain is seen in the SEM images [Figs. 9(a) and (b)], which indicate a composition variation on the grain surface. This appearance is different from that of the LSCF pellet before annealing and shown in Fig. 6(a). The difference already indicates a surface instability of the LSCF pellet. While for the LSM-coated LSCF, the high local contrast seen on the bare and annealed LSCF is absent, as shown in the Figs.9(c) and (d). Chemical compositions of a dark area as well as a white area of bare LSCF annealed at 850°C for 900 h were examined using EDS attached to the SEM and the energy spectra are shown in Figs. 9(e) and (f). This pair of EDS spectra were acquired with identical parameters. As shown in Figs. 9(e) and (f), higher counts of Sr and O are seen in the dark area than the white area. Therefore, surface of the dark area can be enriched in Sr compared with the white area. In contrast, no Sr segregation was observed on the surface of an LSM-coated LSCF after annealing at 850°C for 900 h.[19]

IV. Conclusions

A sol–gel process has been developed for the deposition of LSM films on a dense substrate with precise control of thickness, morphology, microstructure, and composition. The use of a mixed organic solvent of 2-methoxyethanol and acetic acid is necessary to achieve the required stability and wettability of the LSM sols for film deposition on LSCF substrates. The thickness of the LSM films can be controlled within the range of 5–60 nm by spin-coating with different sol concentrations. Annealing at 800°C for 1 h is sufficient to develop the desired LSM perovskite phase on dense

substrates and LSM films grow epitaxially on LSCF grains due to their structural similarity. While local Sr-enrichment was detected on the surface of LSCF pellet after annealing at 850°C for 900 h, a thin film coating of LSM on an LSCF pellet might have successfully suppressed the Sr-enrichment on LSCF surface, implying that an LSM-coated LSCF may have better stability in structure, composition, and morphology under typical SOFC operating conditions.

Acknowledgments

This material is based upon work supported as part of the DOE SECA Core Technology Program under Award Number DE-NT0006557, the HetroFoaM Center, an Energy Frontier Research Center funded by the U.S. Department of Energy, Office of Science, Office of Basic Energy Sciences under Award Number DE-SC0001061, and the WCU project of the South Korean Government. The authors acknowledge the use of Oak Ridge National Laboratory's SHaRe User Facility, which is sponsored by the Scientific User Facilities Division, Office of Basic energy Sciences, Office of Science, the U.S. Department of Energy.

References

[1]S.C. Singhal, "Advances in Solid Oxide Fuel Cell Technology," *Solid State Ionics*, **135** [1–4] 305–13 (2000).

[2]L. Yang, S. Wang, K. Blinn, M. Liu, Z. Liu, Z. Cheng, and M. Liu, "Enhanced Sulfur and Coking Tolerance of a Mixed Ion Conductor for SOFCs: $BaZr_{0.1}Ce_{0.7}Y_{0.2-x}Yb_xO_{3-d}$," *Science*, **326** [5949] 126–9 (2009).

[3]Z. Shao and S. M. Haile, "A High-Performance Cathode for the Next Generation of Solid-Oxide Fuel Cells," *Nature*, **431** [7005] 170–3 (2004).

[4]C. Xia and M. Liu, "Novel Cathode for Low-Temperature Solid Oxide Fuel Cells," *Adv. Mater.*, **14** [7] 521–3 (2002).

[5]P. Singh and N. Q. Minh, "Solid Oxide Fuel Cells: Technology Status," *Int. J. Appl.Ceram. Tech.*, **1** [1] 5–15 (2004).

[6]E. P. Murray, T. Tsai, and S. A. Barnett, "Oxygen Transfer Processes in (La,Sr)MnO3/Y2O3-stabilized ZrO2 Cathodes: An Impedance Spectroscopy Study," *Solid State Ionics*, **110** [3–4] 235–43 (1998).

[7]S. P. Simmer, M. D. Anderson, M. H. Engelhard, and J. W. Stevenson, "Degradation Mechanisms of La–Sr–Co–Fe–O_3 SOFC Cathodes," *Electrochem. Solid-State Lett.*, **9** A478–81 (2006).

[8]J.-Y. Kim, V. L. Sprenkle, N. L. Canfield, K. D. Meinhardt, and L. A. Chick, "Effects of Chrome Contamination on the Performance of $La_{0.6}Sr_{0.4}Co_{0.2}Fe_{0.8}O_3$ Cathode Used in Solid Oxide Fuel Cells," *J.Electrochem. Soc.*, **153**, A880–6 (2006).

[9]S. Li, W. Jin, P. Huang, Na. Xu, J. Shi, and Y. S. Lin, "Tubular Lanthanum Cobaltite Perovskite Type Membrane for Oxygen Permeation," *J. Membrane Sci.*, **166** [1] 51–61 (2000).

[10]A. Thursfield and I. S. Metcalfe, "Air Separation using a Catalytically Modified Mixed Conducting Ceramic Hollow Fibre Membrane Module," *J. Membrane Sci.*, **288** [1–2] 175–87 (2007).

[11]J. A. Lane, S. J. Benson, D. Waller, and J. A. Kilner, "Oxygen Transport in La0.6Sr0.4Co0.2Fe0.8O 3−δ," *Solid State Ionics*, **121** [1–4] 201–8 (1999).

[12]M. Prestat, J. F. Koenig, and L. J. Gauckler, "Oxygen Reduction at Thin Dense La0.52Sr0.48Co0.18Fe0.82O 3−δ Electrodes. Part I: Reaction Model and Faradaic Impedance," *J. Electroceram.*, **18** [1–2] 87–101 (2007).

[13]J.-W. Lee, Z. Liu, L. Yang, H. Abernathy, S.-H. Choi, H.-E. Kim, and M. Liu, "Preparation of Dense and Uniform $La_{0.6}Sr_{0.4}Co_{0.2}Fe0.8O_{3-\delta}$ (LSCF) Films for Fundamental Studies of SOFC Cathodes," *J. Power Sources*, **190** [2] 307–10 (2009).

[14]Y. Choi, M.C. Lin, and M. Liu, "Rational Dsign of Novel Cathode Materials in Solid Oxide Fuel Cells using First-Principles Simulations," *J. Power Sources*, **195** [5] 1441–5 (2010).

[15]Z. Liu, M. Liu, and M. Liu, "LSM-Infiltrated LSCF Cathodes for SOFCS," under review

[16]C. J. Fu, K. N. Sun, X. B. Chen, N. Q. Zhang, and D. R. Zhou, "Electrochemical Properties of A-site Deficient SOFC Cathodes under Cr Poisoning Conditions," *Electrochim. Acta.*, **54** [28] 7305–12 (2009).

[17]G. W. Kauffman and P. C. Jurs, "Prediction of Surface Tension, Viscosity, and Thermal Conductivity for Common Organic Solvents Using Quantitative Structure−Property Relationships," *J. Chem. Inf. Comput. Sci.*, **41** [2] 408–18 (2001).

[18]Y. Huang, J. M. Vohs, and R. J. Gorte, "Characterization of LSM-YSZ Composites Prepared by Impregnation Methods," *J. Electrochem. Soc.*, **152** [7] A1347–53 (2005).

[19]M. Lynch, L. Yang, W. Qin, J.-J. Choi, M. F. Liu, K. Blinn, and M. Liu, "Enhancement of La0.6Sr0.4Co0.2Fe0.8O3-δ Durability and Surface Electrocatalytic Activity by La0.85Sr0.15MnO3-δ Investigated using a New Test Electrode Platform," *Energy Environ. Sci.*, accepted.

[20]G. Anandakumar, N. Li, A. Verma, P. Singh, and J.-H. Kim, "Thermal Stress and Probability of Failure Analyses of Functionally Graded Solid Oxide Fuel Cells," *J. Power Sources*, **195** [19] 6659–70 (2010). □